Supplementary Materials for

3D architecture and complex behavior along the simple central San Andreas fault

Yifang Cheng *et al.*

*Corresponding author. Email: chengyif@berkeley.edu

This PDF file includes:

Figs. 1 to 12

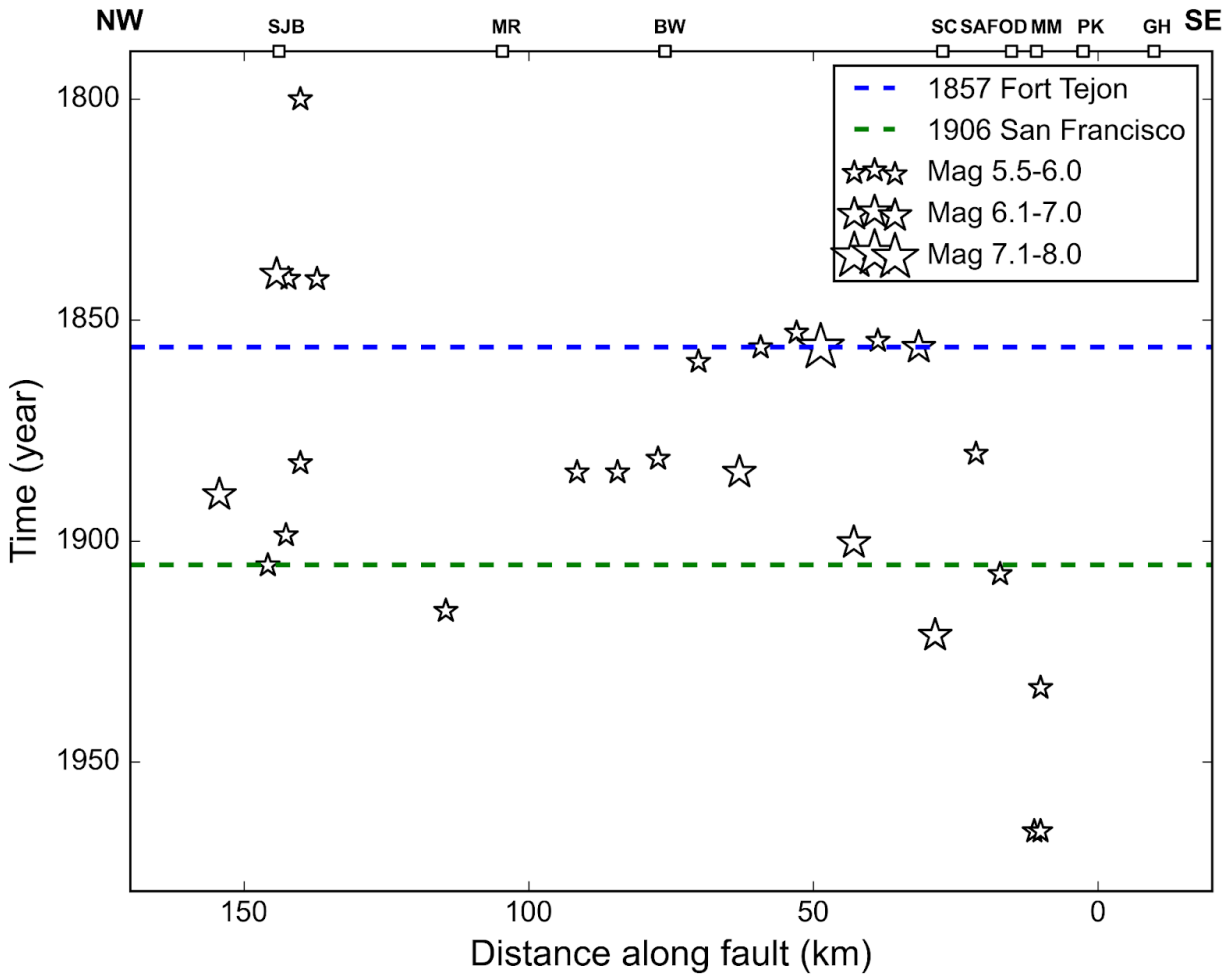

Fig. 1. Spatiotemporal distribution of historical $\boldsymbol{M_w \geq 5.5}$ earthquakes before 1984 presumed to have occurred on the CSAF from Toppozada et al., (2002).

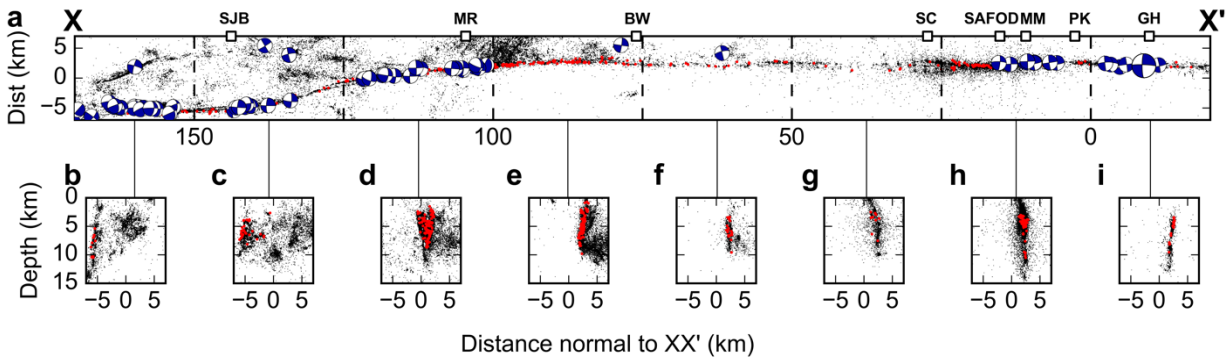

Fig. 2. a Rotated map view, **b-i** cross-section views of seismicity (black dots), M4.0 earthquakes (blue beachballs), and repeating earthquakes (Waldhauser and Schaff, 2021; red dots) along the Central San Andreas Fault. The local coordinate system has its origin at latitude 35.867°N, longitude 120.447°W and is oriented N42°W. SJB: San Juan Bautista, MR: Melendy Ranch; BW: Bitterwater; SC: Slack Canyon; SAFOD: San Andreas Fault Observatory at Depth; MM: Middle Mountain; PK: Parkfield; GH: Gold Hill.

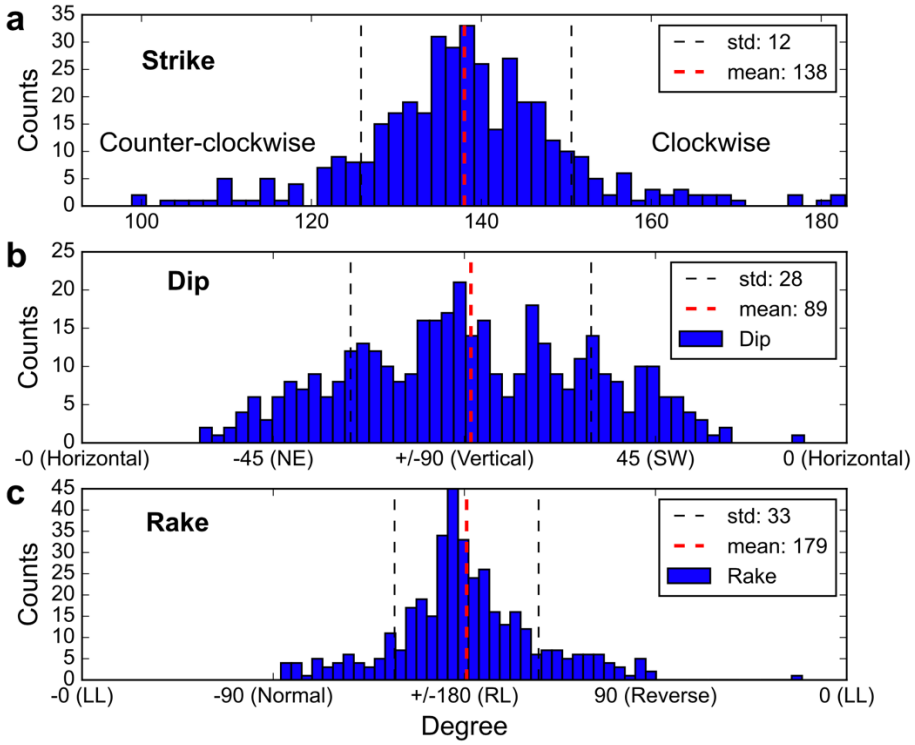

Fig. 3. Histogram of the **a** strike, **b** dip, and **c** rake of the preferred nodal plane of the repeating earthquake sequences with smaller azimuthal difference from the main-fault, N42°W-striking orientation. Red and black dashed vertical lines denote the mean and one standard deviation, respectively.

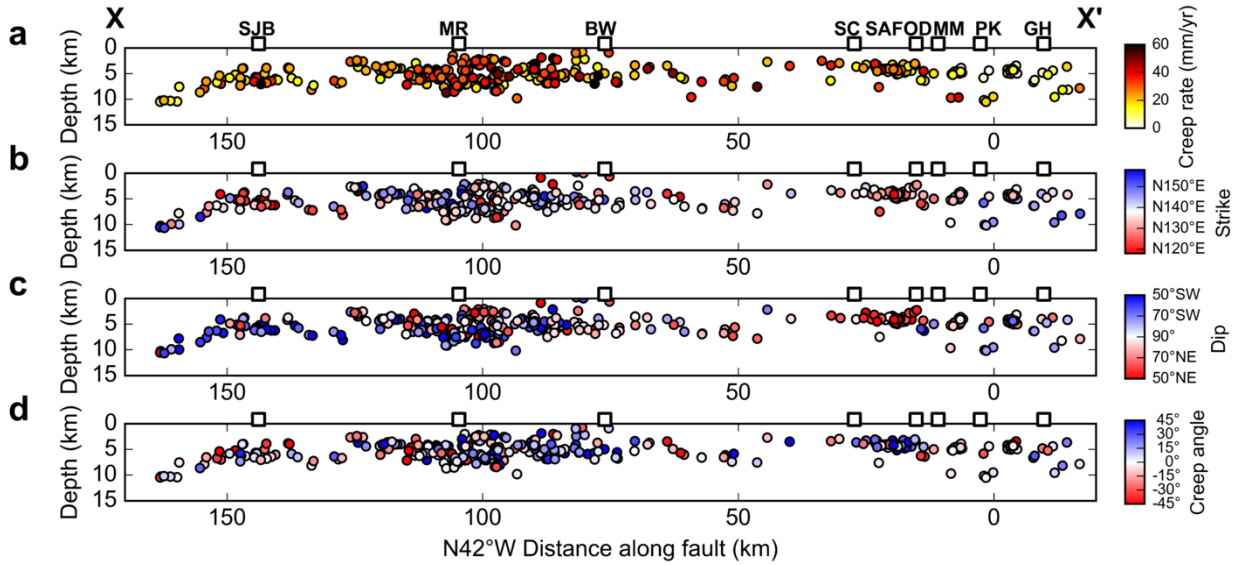

Fig. 4 Cross-section view of repeating earthquake sequences colored by **a** creep rate estimated from occurrence rate, **b** preferred strike angle, **c** dip angle, and **d** creep direction estimated from their focal mechanism. The data in **a** and **d** are used to estimate the creeping rate and direction in each fault patch in Fig 4**c** and 4**e in the main text**, respectively. Positive creep directions indicate a NE-side-up dip-slip component.

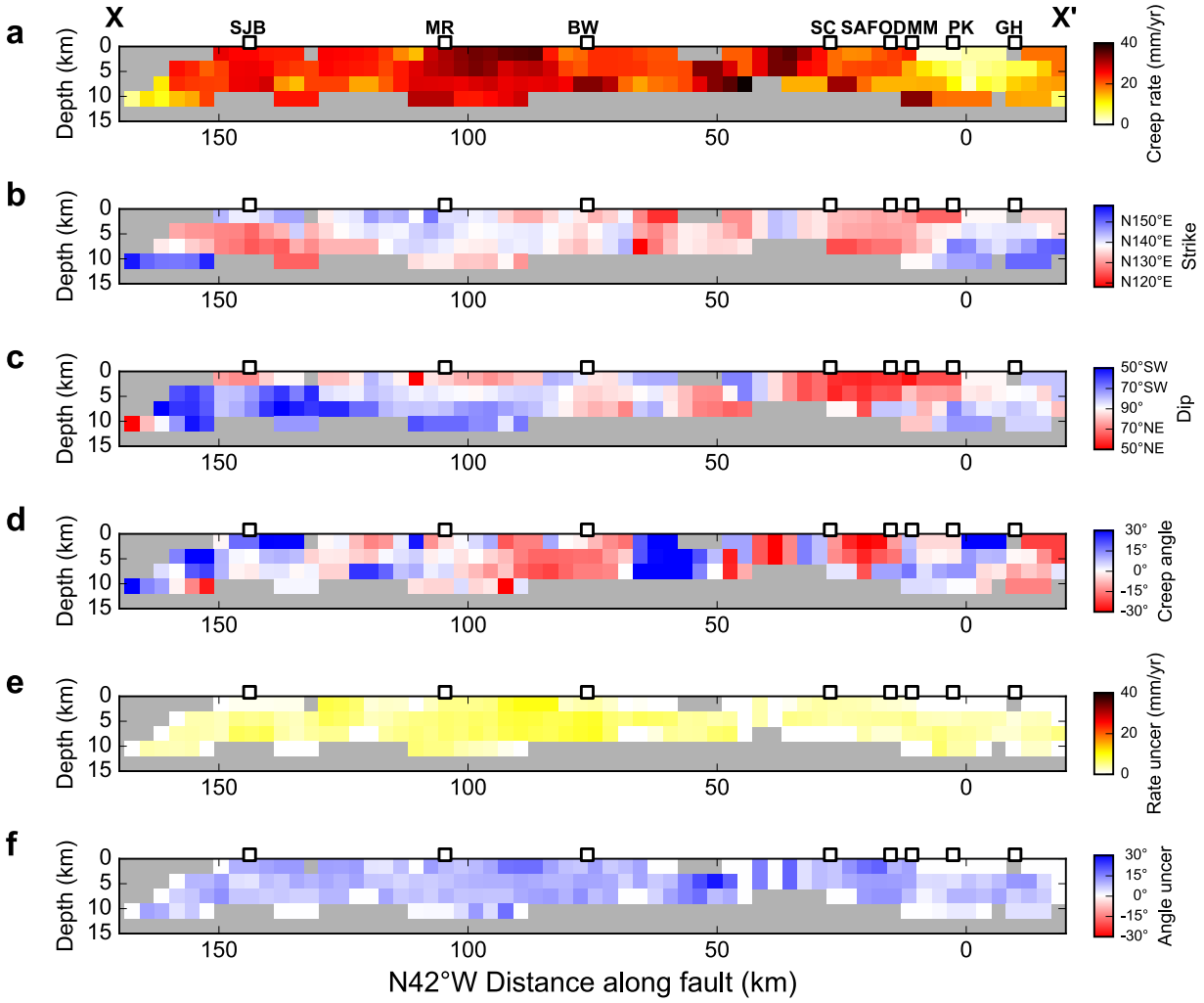

Fig. 5 Spatial variation of the fault creep rate, strike, dip, and creep direction estimated from repeating earthquakes on each fault patch (See Fig. 4 in the main text). The size of each fault patch is 3×3 km. Positive creep directions indicate a NE-side-up dip-slip component.

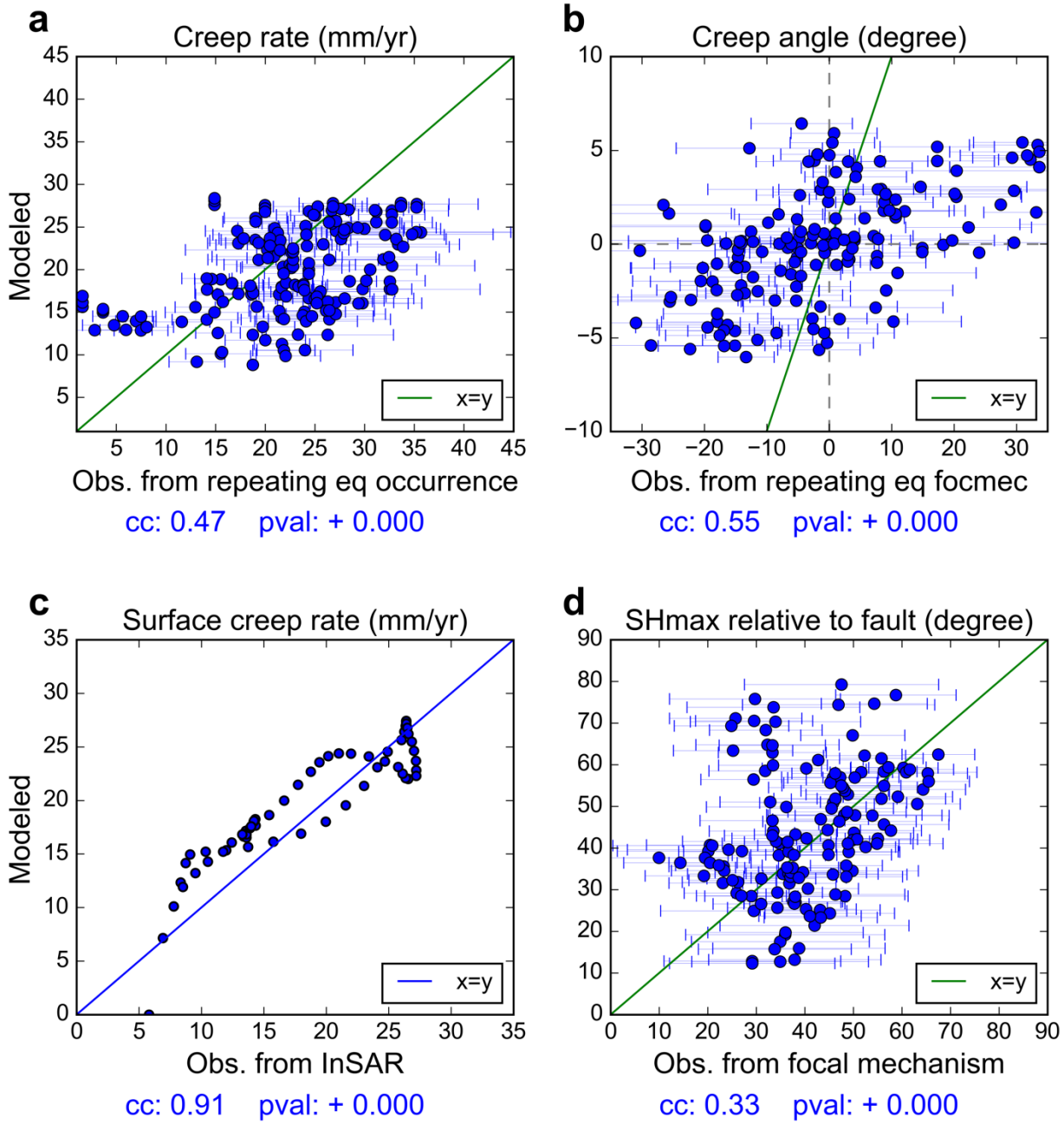

Fig. 6 Point-to-point comparisons of the **a** slip rate, **b** slip direction, **c** surface creep rate, and **d** the angle between main fault and the off-fault maximum horizontal stress orientation (θ) (from the area 1.5 km NE to the main fault) modeled from the fault coupling model A (Y-axes) and those estimated from **a** repeating earthquake occurrence rates, **b** repeating earthquake focal mechanisms, **c** InSAR data, and **d** $M_l \geq 1.0$ focal mechanisms (X-axes). (See Figs 4, 5b, and 5c in the main text for the data used for comparison)

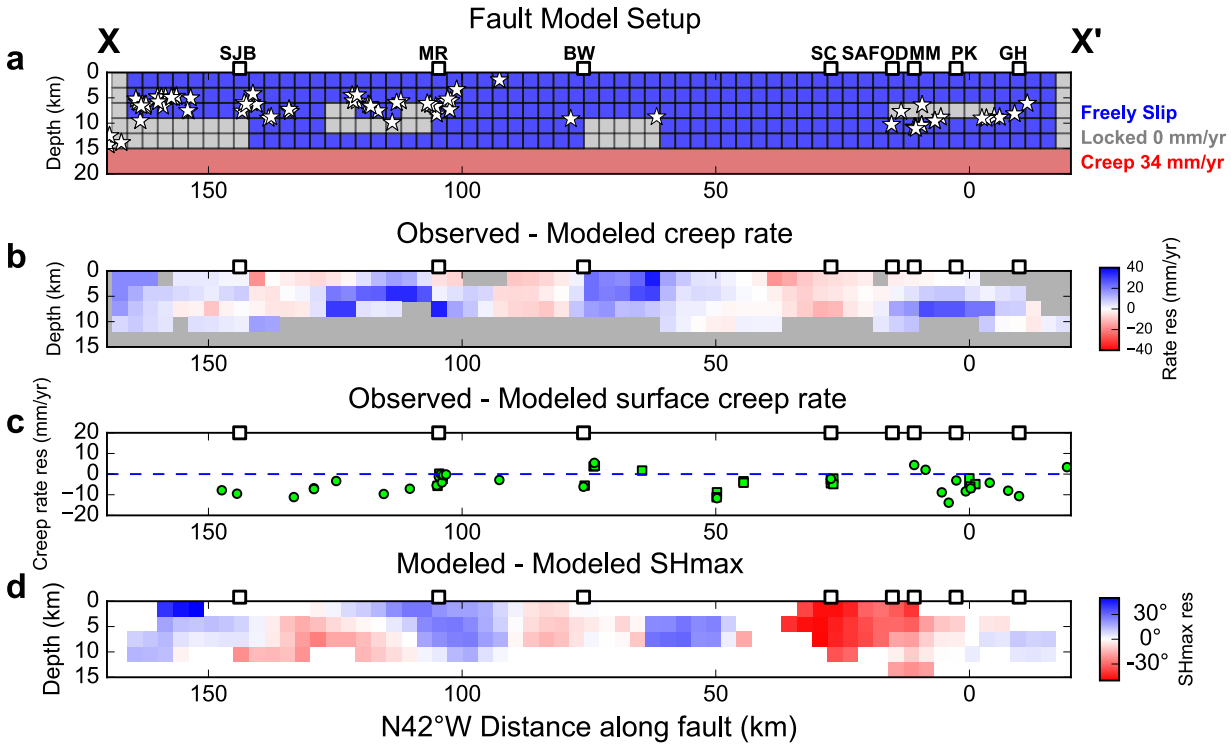

Fig. 7 Residuals between the observed and modeled **b** fault creep rate at depth, **c** surface creep rate, and **d** fault creep direction from **a** fault coupling model A (see Fig. 4 and Fig. 5 in the main text).

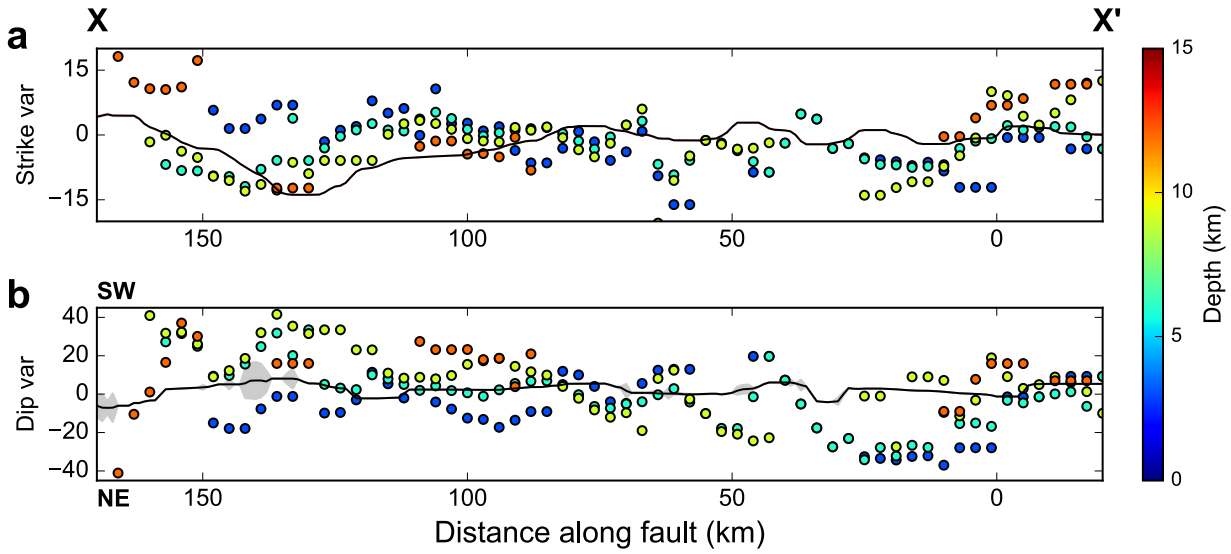

Fig. 8 Comparisons of main fault **a** strike and **b** dip angles estimated from seismicity (Fig 2; black line) and the focal mechanisms of repeating earthquake sequences (fig. S4, B and C; colored dots). The gray areas denote the uncertainty of the estimated strike and dip orientation from seismicity. The focal mechanisms of repeating earthquake sequences have uncertainties (one standard deviation of a set of acceptable focal mechanisms considering the actual focal mechanism variations in each sequence and the expected errors in input data) less than 25 degrees.

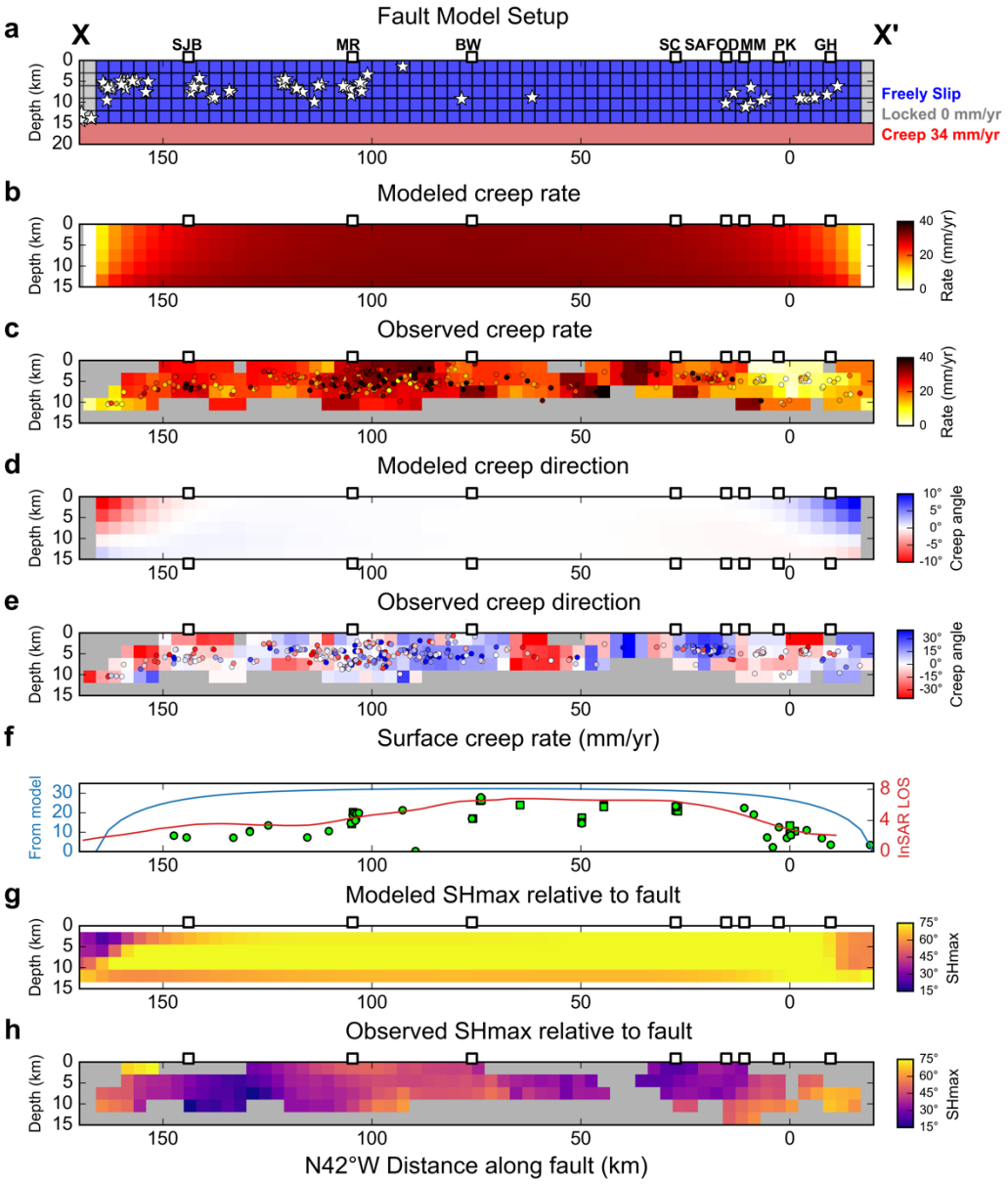

Fig. 9 a Fault model B setup of a fully uncoupled CSAF with freely slipping zones (blue), locked sections (gray) and steadily creeping zones (red). The shallow fault is fully coupled beyond 166 km NW and -17km SE of the fault. The size of each fault patch is 3×3km. White stars denote $M_l \geq 4.0$ earthquakes. **b** Modeled and **c** observed fault creep rate estimated from the occurrence of repeating earthquakes. **d** Modeled and **e** observed fault creep direction estimated from the rake and dip of repeating earthquake focal mechanisms. Positive creep directions indicate a NE-side-up dip-slip component. **f** Modeled (blue) and observed surface creep rate (red) estimated from InSAR data (Jolivet et al., 2014), creepmeters (green circles) and alignment arrays (green squares) (Titus et al., 2006). **g** The angle between the main fault and the modeled off-fault maximum horizontal stress orientation (θ) (from the area 1.5km NE of the main fault). **h** The angle between the main fault and the observed maximum horizontal stress orientation calculated from M1.0 focal mechanisms located within 2km around the fault trace.

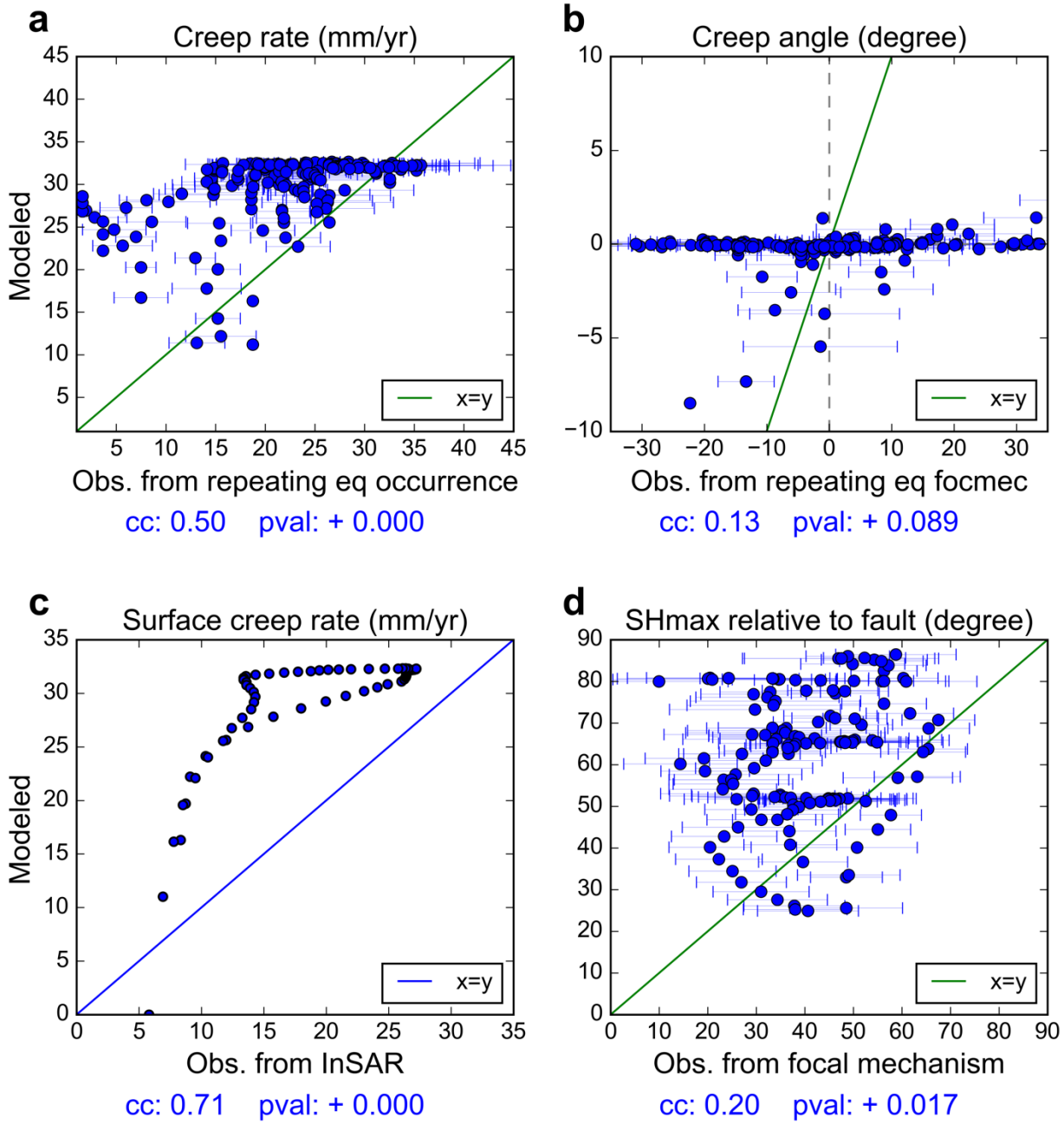

Fig. 10 Point-to-point comparisons of the **a** slip rate, **b** slip direction, **c** surface creep rate, and **d** the angle between main fault and the off-fault maximum horizontal stress orientation θ (from the area 1.5km NE to the main fault) modeled from the fault coupling model B (Y-axes) and those estimated from **a** repeating earthquake occurrence rates, **b** repeating earthquake focal mechanisms, **c** InSAR data, and **d** M1.0 focal mechanisms (X-axes). (See Fig. 9 for the data used for comparison)

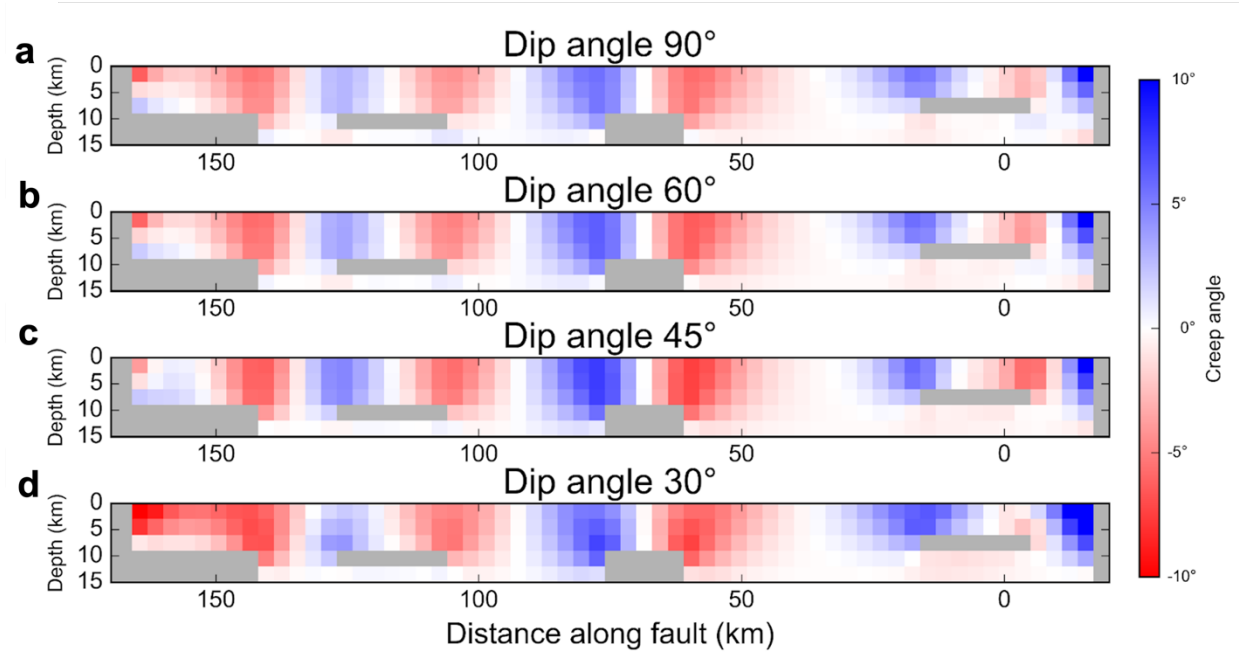

Fig. 11 Modeled fault creep direction using fault model A with different, but uniform, SW dip angles. Positive creep directions indicate a NE-side-up dip-slip component.

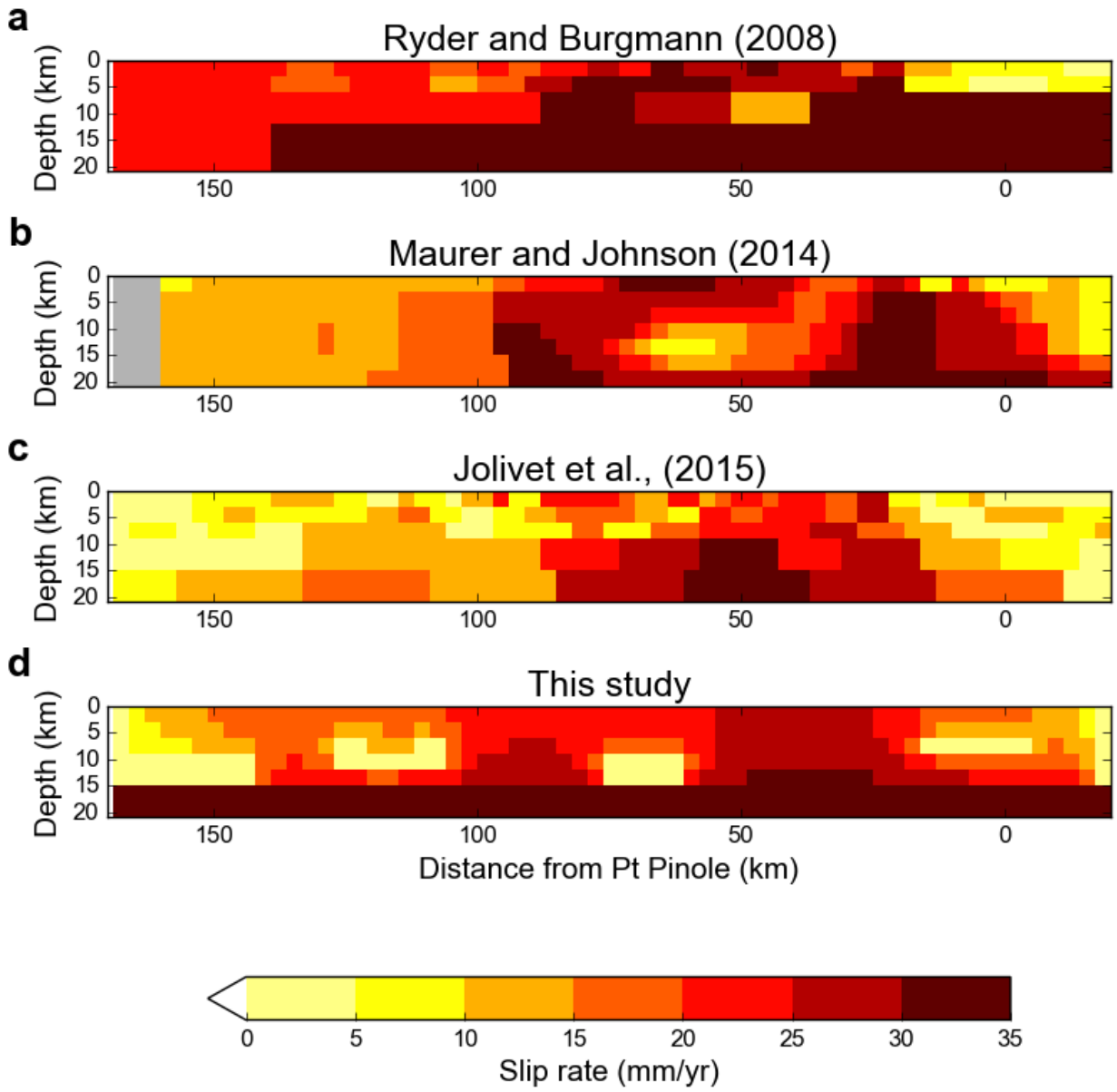

Fig 12. Comparison of several fault coupling models on the central San Andreas Fault. Collection of the modeled distributions of subsurface inter-seismic fault slip rate on the CSAF from (a) Ryder and Bürgmann (2000), (b) Maurer and Johnson (2014), (c) Jolivet et al., (2015), and (d) this study. All models shown at the same spatial and color sale.